Design of a Contact-Aided Compliant Notched-Tube Joint for Surgical Manipulation in Confined Workspaces

Eastwood, Kyle W.
Center for Image Guided Innovation and Therapeutic Intervention (CIGITI),
The Hospital for Sick Children, 555 University Avenue, Toronto, Ontario, Canada, M5G 1X8
kyle.eastwood@mail.utoronto.ca

Francis, Peter
Center for Image Guided Innovation and Therapeutic Intervention (CIGITI),
The Hospital for Sick Children, 555 University Avenue, Toronto, Ontario, Canada, M5G 1X8
peter.francis@mail.utoronto.ca

Hamidreza Azimian
Senior Robotics Researcher at Epson
Epson Canada Ltd, 185 Renfrew Drive
Markham, Ontario, Canada, L3R 6G3
hamidreza.azimian@ea.epson.com

Swarup, Arushri
Center for Image Guided Innovation and Therapeutic Intervention (CIGITI),
The Hospital for Sick Children, 555 University Avenue, Toronto, Ontario, Canada, M5G 1X8
arushri.swarup@mail.utoronto.ca

Looi, Thomas
Center for Image Guided Innovation and Therapeutic Intervention (CIGITI),
The Hospital for Sick Children, 555 University Avenue, Toronto, Ontario, Canada, M5G 1X8
thomas.looi@sickids.ca

Drake, James M. [1]
Division of Neurosurgery, Center for Image Guided Innovation and Therapeutic Intervention (CIGITI), The Hospital for Sick Children, 555 University Avenue, Toronto, Ontario, Canada, M5G 1X8
james.drake@sickkids.ca

Naguib, Hani E.
Smart and Adaptive Polymers Laboratory (SAPL), Department of Mechanical and Industrial Engineering, University of Toronto, 5 King's College Road, Toronto, Ontario, Canada, M5S 3G8
naguib@mie.utoronto

[1] Corresponding author

ABSTRACT

This work presents a novel miniature contact-aided compliant joint mechanism that can be integrated into millimeter-sized manual or robotic surgical instruments. The design aims to address the trade-off between notched-tube compliant joints' range-of-motion and stiffness, while also ensuring a compact form-factor. The mechanism is constructed from a nitinol tube with asymmetric cutouts and is actuated in bending by a cable. The innovative feature of this design is the incorporation of a contact-aid into the notched-tube topology which acts to both increase the stiffness of the joint and change the shape that it undertakes during bending. Using finite element modelling (FEM) techniques, we present a sensitivity analysis investigating how the performance of this contact-aided compliant mechanism (CCM) is affected by its geometry, and derive a kinematics and statics model for the joint. The FEM simulations and the kinematic and static models are compared to experimental results. The design and modelling presented in this study can be used to develop new miniature dexterous instruments, with a particular emphasis on applications in minimally invasive neurosurgery.

1 INTRODUCTION

Notched-tube compliant joint mechanisms have increasingly been used to construct miniature dexterous medical instruments, such as articulated fiber-optic endoscopic cameras, articulated lasers, suction and irrigation probes, as well as wristed forceps, scissors and drills [1]–[10]. More recently, a particular focus on adopting this technology for endoscope-guided neurosurgery (neuroendoscopy), to create dexterous wristed instruments, has emerged [1]–[7]. For these applications, the instruments are typically 1-2 millimeters in diameter and are used to operate within confined workspaces whose dimensions vary in the 5-20 mm range [8]. Notched-tube joints are constructed by cutting macro-scale patterns into metal tubes, and can be fabricated in a single process from a single material. In their simplest form, these monolithic geometries can be articulated in bending using an actuation cable, requiring minimal assembly and few additional components. These features allow for this type of joint to be manufactured at millimeter sizes, and for these reasons, they are frequently favored over pin-jointed mechanisms when constructing tools for working in confined body cavities. However, when designing these devices for operating in millimeter-sized workspaces, there is a major design trade-off between joint range-of-motion, joint stiffness and joint compactness.

Some existing notched-tube topologies are depicted in Figure 1-A. These designs can be classified as either asymmetric or symmetric, and different combinations of notches create different degrees-of-freedom (DOF) and directions of bending. Asymmetric notch topologies have been found to achieve more compact bending compared to symmetric designs because they fold into themselves during articulation. The simplest notch topology that has been reported is rectangular in shape as shown in design *i* [1], [9]–[11]. Over time, additional features have been

proposed to modify this basic topology to improve its performance. One such feature includes changing the notch shape to prevent the joint from reaching the material's elastic strain limit by tapering the notches, shown in designs *ii* and *v* [12], [13]. A second common feature includes adding fillets to the corners of the notch, or rounding the notch, to reduce strain concentrations at these locations, as seen in *ii*, *iii* and *v* [12], [14]–[16]. As well, the concept of "tip-first-closure" was recently explored which involves varying the depth of cut of the notches so that the most distal end of the joint articulates closed before the more proximal notches [2]. These modifications have improved the strain profile within the joint and have also helped to ensure the mechanism bends in a compact and space-efficient shape. However, as this type of mechanism is scaled below the 1-2 mm diameter range, the joint's stiffness is significantly reduced. Achieving a joint that is both compact and simultaneously stiff enough to manipulate tissue is a major challenge.

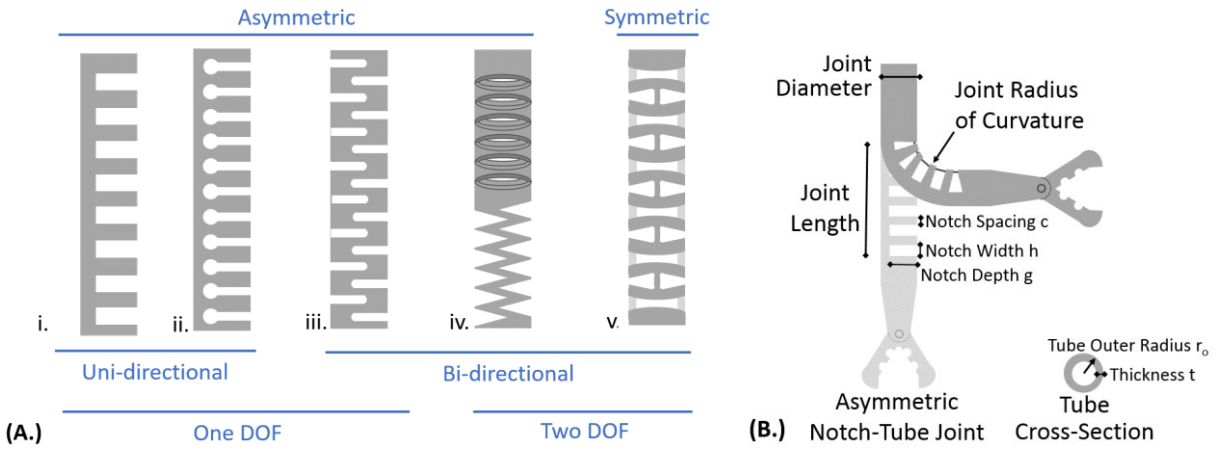

Figure 1: Notched-Tube Topologies Previously Reported for Medical Devices [1]–[3], [9]–[11], [13], [15]–[19] (A). Examples of Notch Topology Incorporated into Surgical Forceps with Notation Used to Define Joint Geometry (B).

Figure 2 depicts different external forces that could be applied to an asymmetric notched-tube joint by manipulating tissue. Loads applied along the x-axis (F_x^+ and F_x^-) result in significantly

lower “error-motions” (undesired deflections) compared to loads applied along the y-axis because of the second-moment of area of the joint in this orientation. Along the y-axis, where the second-moment and stiffness of the joint is much lower, loads such as F_y^- can be opposed by tensioning the actuation cable, however, significant error-motions occur when loads are applied in the F_y^+ direction. The current strategies used to address this problem focus on increasing the joint’s overall stiffness, and unfortunately tend to oppose the strategies used to achieve compact bending. According to [2] and [3], decreasing the joint’s tube diameter and increasing the notch depth appear to have the most significant impact on the compact bending of individual notches, but these strategies also significantly reduce stiffness. This work aims to address the trade-off between compactness and stiffness for conventional topologies by introducing the use of “contact-aids” into the design of asymmetric notched-tube compliant mechanisms.

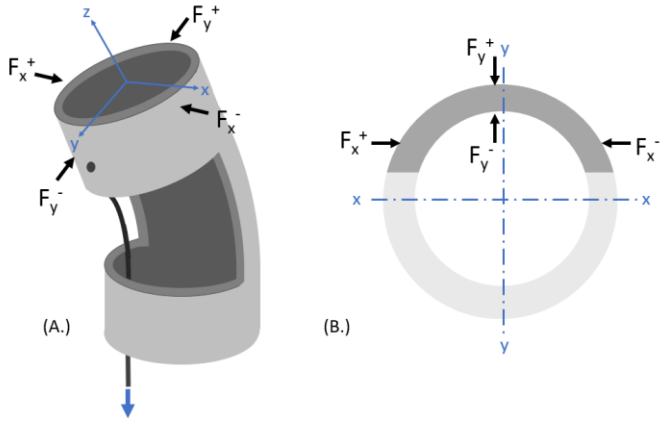

Figure 2: Notched-Tube Segment with Externally Applied Loads (A). Cross-Section of Tube Notch (B).

Contact-aided compliant mechanisms (CCMs) are a category of joint designs in which parts of the compliant members contact or interfere with one another to improve the mechanisms’ performance [19]. These joint designs have been studied extensively and have shown promise in aerospace, medical and biomimetic inspired robotics applications [20]–[23]. In

particular, CCMs have been used to affect the "shape" that the compliant mechanism undertakes during actuation, and separately, CCMs have been employed to increase the directional stiffness of a compliant joint [20]. This work presents a new CCM notched-tube cutting geometry that was developed to increase the compact bending of asymmetric notch designs by changing their shape while articulating, and simultaneously, increasing the tip loads that the joint can support, without excessive deflection, during articulation. To the best of our knowledge, this work presents the first example of a CCM incorporated into a notched-tube compliant mechanism. We begin by presenting an overview of the joint topology and the performance benefits of the design. Then, we describe the development of a CCM notch joint for neurosurgical tool applications. Here, finite-element modelling (FEM) techniques have been used to study the impact that the contact-aid geometry has on the joint's performance, and to inform the development of a physical prototype. Next, we propose kinematics and statics models to predict the behavior of the joint and guide future prototype optimization and development. Following the modelling, we outline the methods used to fabricate the prototype joints, and describe the experimental techniques used to quantify their performance. Finally, the experimental results are discussed and compared to the FEM, kinematic and statics models.

2 PROPOSED DESIGN OF CCM NOTCHED-TUBE JOINT

The proposed CCM notched-tube joint is an evolution from previous topology features intended to improve upon the basic rectangular notch topology. Where the other features aimed to avoid exceeding strain limits and avoid strain concentrations, this evolution focuses on improving both the stiffness and the compactness of a notched-tube joint. Figure 3 depicts a

design progression showing how the design features were added onto a rectangular notch topology to arrive at the finalized notch prototype.

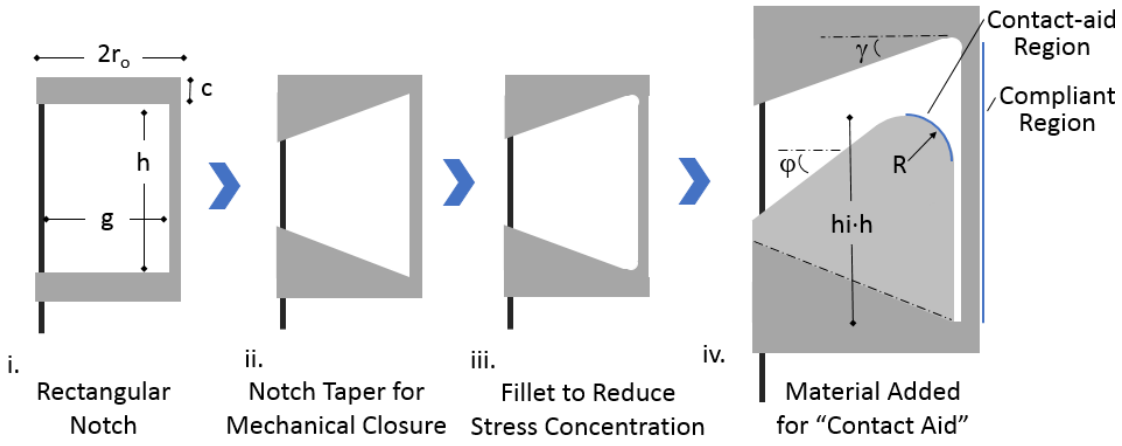

Figure 3: Panel Depicting How Additional Design Features are Added to a Rectangular Notch to Improve Performance. Variables Used to Define the Geonetry are Noted.

Here, the CCM notch topology is configured such that the region of the joint undergoing elastic deformation (compliant joint region) comes into point contact with a rigid region (contact-aid region) as it articulates. The shape of the notch is designed such that in the presence of an external tip loading force, as depicted in Figure 4-A, the joint is stiffened or self-reinforced, and yet bending of the joint is still permitted when a moment is applied by the actuation cable. For rectangular asymmetric notches, external forces applied in the direction shown in Figure 4-A result in the largest displacements. This result occurs because the second-moment of area of the compliant region is the smallest in this orientation and because the applied load cannot be opposed by the actuation cable. The CCM topology aims to address this vulnerability for asymmetric notches by reinforcing the compliant region, as seen in Figure 4-A. Incorporating the contact-aid also influences the shape of the notch's compliant region when actuated. The joint's compliant region takes on an elliptical shape, as opposed to a circular arc, while bending which allows the joint to bend in a more compact form-factor with less lateral movement. These

benefits of improved stiffness and bending compactness are illustrated in Figure 4 which was generated using FEM and is included here for illustrative purposes. Figure 4-A depicts how the stiffness increases when the compliant region touches the contact-aid, and the slope of the force-deflection curve changes from K_1 to K_2. Figure 4-B depicts the percent reduction in lateral motion of the top edge of the joint for different contact-aid geometries (h_i) when the notch is fully articulated to 30°.

The trade-offs introduced with this design, which include an increase in cable tension and increased strain around the contact-aid, will be considered as part of the sensitivity study for this topology in section 3.2.

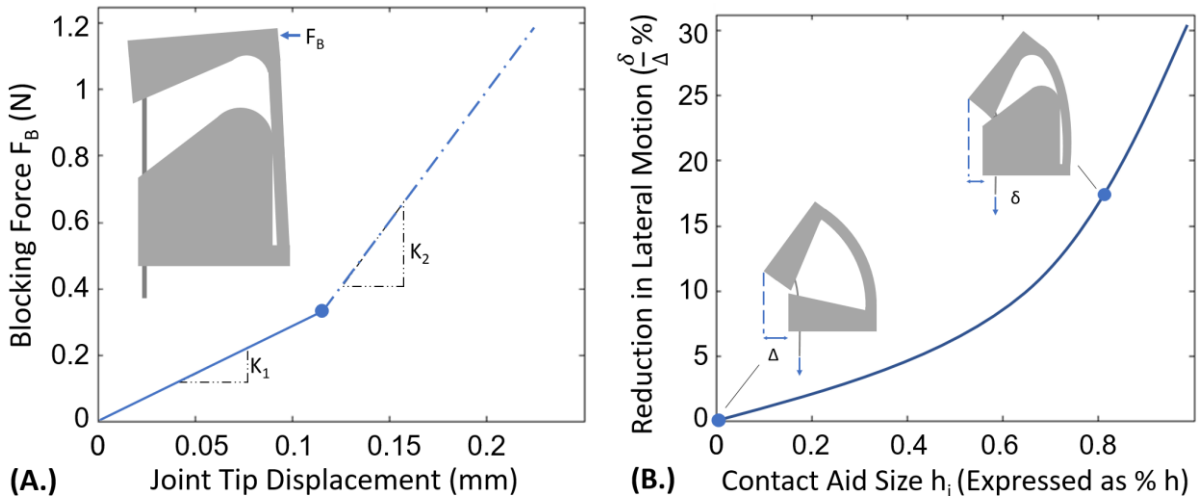

Figure 4: Illustrative Example Demonstrating the Behavior of a Theoretical Contact-Aided Notched-tube Compliant Joint Compared to a Rectangular Notched-tube That Does Not Have the Contact-Aid Added

3 PROTOTYPE DEVELOPMENT WITH A FOCUS ON NEUROENDOSCOPIC INSTRUMENT DESIGN

To demonstrate an application of the CCM notched-tube joint, it has been incorporated into a neurosurgical instrument shaft to add wrist-like motion for operating within the ventricles of the brain. With the benefits provided by the CCM notch, the capabilities of the joint are expected to provide sufficient stiffness for tissue manipulation beyond what was previously

possible. To construct a neuroendoscopic instrument joint that is compatible with commercial ventricuoloscopes, the outer-diameter of the tube should be less than 1.5 mm. For all the joints analyzed in the present work, a tube with an outer-diameter of 1.25 mm and thickness of 0.1 mm was selected to account for any additional covering or sheathing that may be added to the outside of the tube to enclose the notches during surgical use. The physical joints manufactured for this study were constructed from commercially available nickel-titanium (nitinol) tubes (Confluent Medical Technologies Inc., USA). Previous work that focused on optimizing the design of a rectangular notched-tube topology for a neuroendoscopic instrument was presented in [3], and this modelling technique was used as a starting point for selecting the geometry and layout of a multi-segment notched-tube joint for this paper. Previous studies have indicated that selecting the minimum length of spacing (*c*) between the notches will help to achieve the most compact radius of curvature of the joint [1]. Further, using the fewest possible number of deeply cut notches, and maximizing the width of each notch, will also ensure the most compact joint design that can achieve a desired bending angle [2], [3]. These design guidelines were incorporated into the selection of the notched-tube geometry. The contact-aid feature was then subsequently added onto this rectangular geometry. The number of notches *n*, the notch cut depth *g*, the notch width *h* and the notch spacing *c* for a basic asymmetric rectangular topology (Figure 3), onto which the contact-aid is eventually added, are summarized in Table 1. The number of notches were chosen to achieve a desired bending angle of approximately 80 degrees. The geometry specific to the contact-aid design is analyzed using FEM and discussed in the following section.

138 **Table 1: Rectangular Notch Joint Geometry Used as Starting Point for Design**

Joint Parameter	Value
Tube Outer Radius r_o	0.62 mm
Tube Inner Radius r_i	0.52 mm
Notch Cut Depth g	1.00 mm
Notch Width h	1.60 mm
Notch Spacing c	0.62 mm
Notch Fillet Radius	0.2 mm
Number of Notches n	3
Desired Bending Angle	~ 80 Degrees

139

140 **3.1 FINITE ELEMENT MODELLING FOR CONTACT-AID SIZING**

141 A sensitivity study was conducted using the FEM package ANSYS 15.0 Research Version
142 (ANSYS Inc., USA) to inform the sizing of the contact-aid geometry shown in Figure 3. The study
143 explores the impact of varying contact-aid geometry on joint stiffness, bending compactness and
144 maximum equivalent strain. To simulate these effects in the case of typical actuation of the joint,
145 an actuation cable was modelled, fixed to the joint and displaced to reproduce the true behavior
146 of the notch when actuated. The material constitutive model for the joint was implemented as a
147 custom shape memory alloy of super-elasticity type, which is included in the ANSYS engineering
148 data section. The model parameters are outlined in Table 2, and are based on the properties of
149 nitinol provided by the material manufacturer. The constitutive model for the actuation cable,
150 based on stainless steel, is summarized in Table 3.

151 **Table 2: Constitutive Model of Nitinol**

ANSYS Model Parameters	**Value**
Young's modulus of the Austenite phase (E)	55.0 GPa
Poisson's Ratio (ν)	0.3
Material response ratio between tension and compression (α)	0
Maximum residual strain (ε_l)	0.045
Starting stress value for the forward phase transformation (σ_{SAS})	420 MPa
Final stress value for the forward phase transformation (σ_{FAS})	430 MPa

Starting stress value for the reverse phase transformation (σ_{SSA})	220 MPa
Final stress value for the reverse phase transformation (σ_{FSA})	217 MPa

Table 3: Constitutive Model of Steel

ANSYS Model Parameters	Value
Young's Modulus (E)	200 GPa
Poisson's Ratio (ν)	0.3
Yield Stress (σ_{yield})	250 MPa

The model mesh consists of elements of type Solid186, and the mesh size varied in the range of 0.05 mm to 0.15 mm between simulations; this variation was necessary to ensure convergence of a solution. To simulate the attachment between the joint and the actuation cable, a spot weld contact was used, and a frictional contact was specified with a coefficient of friction of 0.3 between the joint's inner surface and the outer surface of the cable. A rigid constraint was implemented to fix the joint's base, and symmetry conditions were applied along the tubes' plane of symmetry so that only half of the model joint was simulated. These constraints are annotated in Figure 5. The parameters defining the geometry of the contact-aid topology are also included.

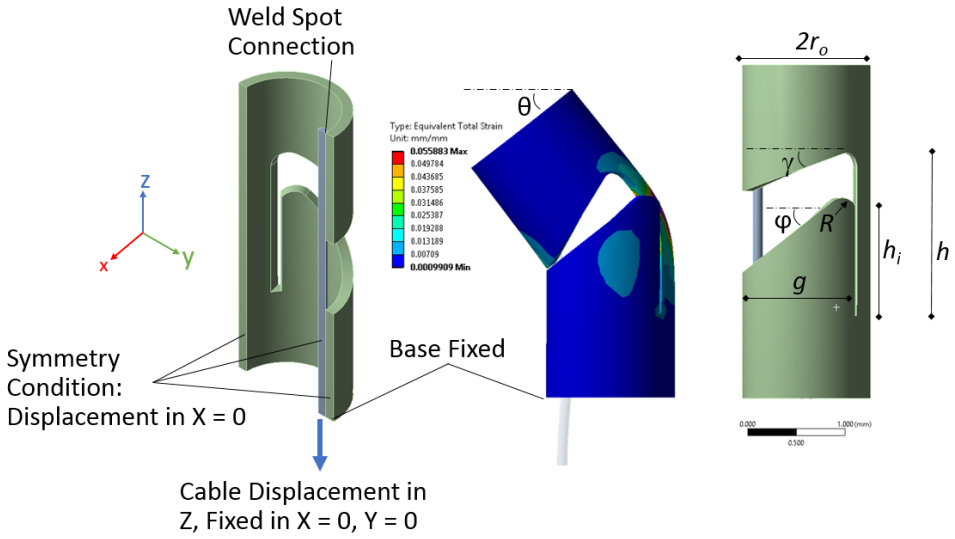

Figure 5: Outline of Finite Element Model Constraints and Boundary Conditions Applied to Simulate the Notch Prototype

The joint was actuated by defining the inferior surface of the cable to displace a predefined amount in a direction parallel to the long axis of the tube. The displacement set-point for a given simulation was estimated to be equal to the notch length *h*. However, in many cases, the maximum principle strain of the tube body reached the elastic strain limit or mechanical closure of the tapered edges occurred before this displacement was reached. Therefore, the articulation angle, the joint's radius of curvature, and the cable-displacement were recorded for all sub-steps. Using this loading configuration, some stretching of the cable occurred. To account for this result, the displacements of the superior and inferior interior edges of the notch were recorded and the Euclidian distance between the edges was calculated. In many cases this value was very close (< 5% discrepancy) to the displacement of the cable.

Both a single notch and a multi-notch joint design were modelled. A frictional contact was also added between cut surfaces on the tube model to simulate the contact-aid. As well, a second static structural simulation was added to the ANSYS workspace to simulate an applied joint-tip blocking force. This simulation was configured to capture the force-deflection characteristics of the joint to estimate the impact of the contact-aid on the joint's blocking-force/stiffness. The loading direction for the force-deflection was along the positive Y-axis in Figure 5.

3.2 SIMULATION RESULTS OF CONTACT AID SIZING

A simulation of one version of the proposed tube topology is depicted in Figure 6-A. The results of a blocking force experiment shown in Figure 6-B demonstrate how the force-deflection is affected by the introduction of the contact-aid. The effective stiffness, denoted *K*, of this notch increased by a factor of approximately 2.2 as indicated by the ratio of the slopes of the force-

deflection curve K_2/K_1. The tip displacement that occurs prior to the shift from K_1 to K_2 is denoted d_c. An optimal design aims to minimize d_c and maximize K_2.

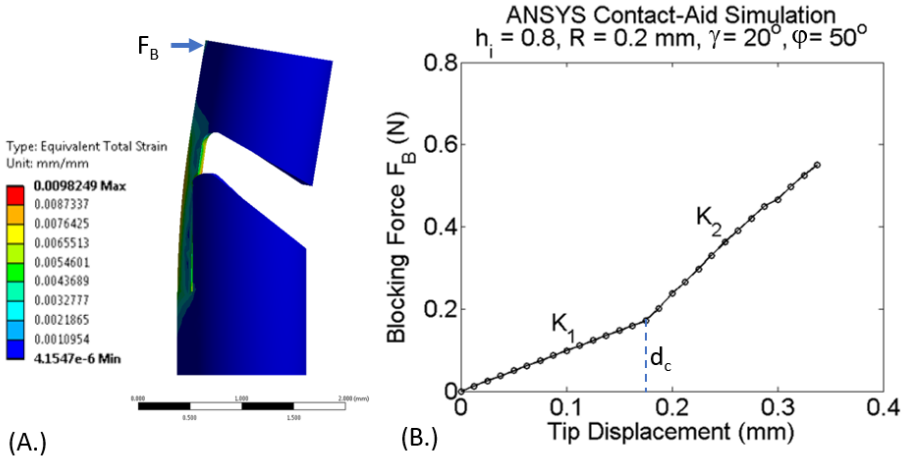

Figure 6: Finite Element Model of Modified Joint showing the Effect of Mechanical Interference on Blocking Force

As outlined in Figure 5, five parameters define the geometry added to the joint to achieve the contact-aid; the contact aid length h_i expressed as a fraction of the notch width h, the top and bottom edge taper angles γ and φ, the slit width s_w, as well as the contact aid radius R. The contact aid length h_i is anticipated to be the most significant topology parameter, and is the focus of the sensitivity study. To investigate how varying h_i impacts the notch stiffness and notch shape during bending, several ANSYS simulations were conducted (Figure 7). These simulations considered both the force-deflection performance and the maximum strain occurring in the joint when articulated to a 30° bending angle. The two taper angles, γ and φ, were held constant at 20 and 50 degrees, respectively, for this study. These angles provide a maximum bending angle of 30° when the joint is fully closed. From early examination, the taper angles do not appear to have a significant effect on the joint's compactness or stiffness characteristics. The slit width s_w theoretically should be set as small as possible, and is therefore determined by fabrication limits

as 0.05 mm, this value will be described in Section 4. The contact radius R impacts strain concentrations but appears to have minimal impact on stiffness changes of the joint. Its value was held constant at 0.2 mm for this study.

Figure 7 attempts to capture the four most significant effects that this new notch design has on the joint's behavior, and how these effects vary with h_i. Increasing h_i results in the compliant region coming into contact with the contact-aid earlier and generally having a more significant impact on the joint's stiffness. For example, topologies where h_i is less than 0.5 experience significantly more tip displacement for a 0.4 N tip load because the joint material begins to undergo a phase transformation from Austenite to Martensite before the contact-aid takes effect and the joint's stiffness increases. Ultimately, higher h_i result in lower values of d_c and higher stiffness for a larger range of applied tip forces. However, introducing the contact-aid also increases the strain of the joint by as much as 2% with this geometry. The 6% strain value is marked as this is the elastic strain limit suggested by the manufacturer. The contact-aid also provides a shape change during actuation which reduces the space that the joint takes up laterally. The reduction of this lateral motion is plotted and shows that it can be reduced up to 25% with the selected geometry. Finally, an increase in the maximum cable actuation tension required to fully articulate the notch is observed as h_i increases.

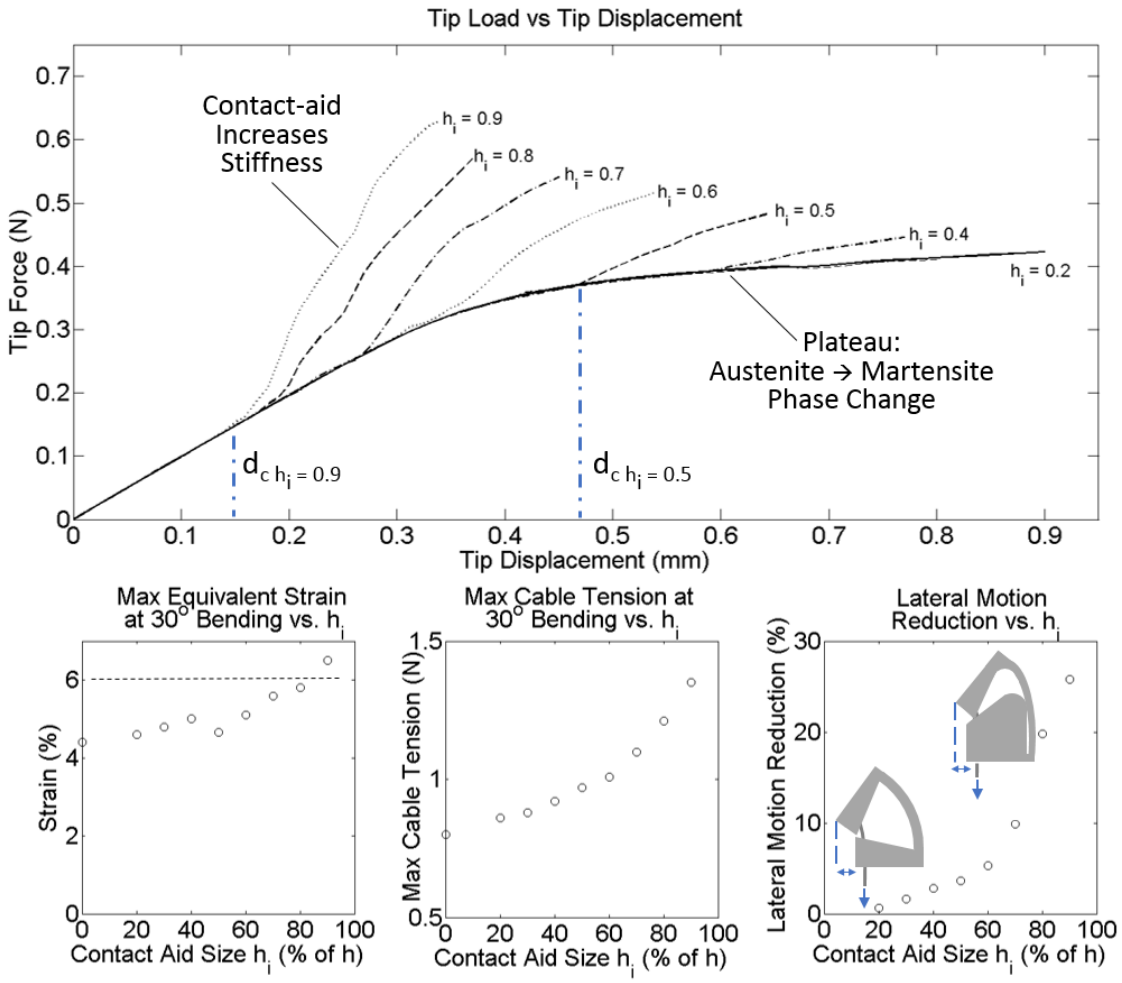

Figure 7: Sensitivity of Stiffness, Max-Strain and Joint Bending Compactness to Contact-Aid Joint Geometry h_i

Based on the simulations, a contact-aid design with h_i of 0.8 was chosen because it gave the best performance in terms of increasing the stiffness and reducing the lateral motion without exceeding 6% strain, which was taken to be the elastic limit. The geometry of the test specimen that were fabricated based on this study are summarized in Table 3.

Table 3: Selected Contact-Aided Joint Parameters (Labelled in Figure 5)

Joint Parameter	Value
Contact Aid Length h_i (% h)	0.8
Top Taper Angle γ	20°
Bottom Taper Angle φ	50°
Slit Width s_w	0.05 mm
Contact Aid Radius R	0.2 mm

4 MODELLING JOINT BEHAVIOR

4.1 KINEMATICS MODELING

In order to predict the relationship between cable displacement and bending angle for this type of joint, an approximate kinematics model was developed based on the geometry of an individual notch. The kinematics model approximates the behavior of the joint by assuming that the majority of bending occurs near the contact-aided region, and that the compliant component of the joint wraps around the filleted edge of the contact-aided region, as shown in Figure 8. The forward kinematics mapping between the input cable displacement and the output joint bending angle is approximated, using the small angle assumption, as follows:

$$\theta \approx \tan^{-1}\left(\frac{\Delta l\,(1+sin\gamma)cos\gamma}{g}\right) \tag{1}$$

where Δl is the input cable displacement for a single notch, θ is the joint tip bending angle, g is the cut depth of the notch and γ is the angle of the top taper as shown in Figure 8.

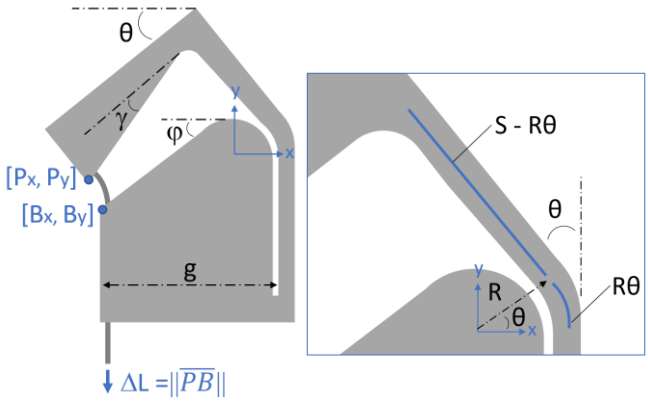

Figure 8: Schematic of Joint Indicating Notation Used in Kinematics Model. For Kinematics a "Simplified" Bending Shape is Assumed where Bending Occurs only at Contact-Aid Region

The inverse kinematics mapping is determined by approximating the locations of the top corner of the notch with coordinates [P_x,P_y] with respect to the bottom corner of the notch with coordinates [B_x, B_y], as follows:

$$P_x - B_x = \overline{PB}_x = g - R\cos(\theta) - (S - R\theta)\sin(\theta) - \left(\frac{g-R}{\cos(\gamma)}\right)\cos(\theta+\gamma) \quad (2)$$

$$P_y - B_y = \overline{PB}_y = R\sin(\theta) + (S - R\theta)\cos(\theta) - \left(\frac{g-R}{\cos(\gamma)}\right)\sin(\theta+\gamma) - R + (g-R)\tan(\varphi) \quad (3)$$

$$\Delta l \approx \left(\overline{PB}_x^2 + \overline{PB}_y^2\right)^{1/2} \quad (4)$$

where $S = (1-h_i)\cdot h$ and φ is the angle of the bottom taper as shown in Figure 8.

4.2 STATICS MODELLING

The cable actuation force required to achieve a desired bending angle can be computed using Castigliano's first theorem:

$$\frac{\partial U(\varepsilon)}{\partial \theta} = M = FL \quad (6)$$

where $U(\varepsilon)$ is the total strain energy stored in the compliant joint, as a function of strain ε, θ is the tip bending angle of the joint and *M* is the bending moment applied to the joint by the actuation cable. This bending moment can be decomposed into the applied cable tension *F* and the moment arm *L*, which is constant and a function of the joint's geometry, expressed as:

$$L = r_i + \bar{y} \quad (7)$$

where r_i is the inner radius of the tube and $\bar{y}$ is the location of the neutral bending plane of the compliant joint. This notation is detailed in Figure 9, and the methods used to compute $\bar{y}$ using the geometry of circular segments is discussed in detail in [3].

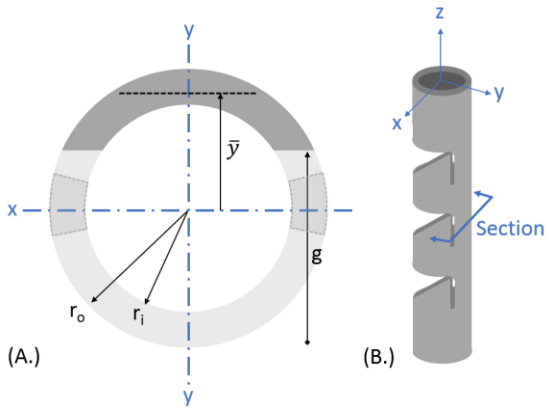

Figure 9: Notation for the Cross-sectional Geometry of a Notched-tube Compliant Joint. The dark section in (A.) is the compliant joint region.

The total strain energy of the joint is computed from the strain energy density $W(\varepsilon) = \int_0^{\varepsilon} \sigma(\epsilon) d\epsilon$, where $\sigma(\epsilon)$ represents the constitutive relationship that maps the stress σ and strain. For nitinol, a piecewise linear stress-strain curve provides a simplified material model that accurately captures the loading of the joint. This model is expressed as:

$$\sigma(\epsilon) = \begin{cases} \sigma_{lp} & \epsilon < \sigma_{lp}/E \\ E\epsilon & \sigma_{lp}/E \leq \epsilon \leq \sigma_{up}/E \\ \sigma_{up} & \epsilon > \sigma_{up}/E \end{cases} \tag{8}$$

To complete this model, a representation of the strain profile within the joint is needed. Assuming that the strain is linearly distributed about the neutral bending plane of the joint $\bar{y}$, the strain profile through a cross-section of the compliant joint is approximated as:

$$\epsilon(t, y) = \frac{k(t)'(\bar{y} - y)}{1 + \bar{y} \cdot k(t)'} \tag{9}$$

Where $k(t)'$ is the bending curvature of the joint at the location $t \in [0,h]$ along the joints arc-length. Up to this point, the procedure for computing the statics model follows the method used in [1] and [2] which was applied to a rectangular shaped notched-tube complaint joint that assumed the notch to take-on a constant curvature bending profile while articulating. For the

contact-aided compliant joint presented in this work, the shape of the compliant bending region of the joint is assumed to take-on an elliptical arc shape. The tip coordinates of an elliptical arc is defined as follows:

$$P_y{}' = B \cdot \sin(\tau) \tag{10}$$

$$A - P_x{}' = A \cdot \cos(\tau) \tag{11}$$

Where the parameters *A* and *B* define the width and height of the ellipse and the parameter τ defines the sweep of the arc. The tip coordinates of the end of the arc are $P_x'(\tau)$ and $P_y'(\tau)$ (Figure 10) which are approximated using the kinematics model as:

$$P_x' = (R\cos(\theta) - R) + (R\theta - S)\sin(\theta) \tag{12}$$

$$P_y' = R\sin(\theta) + (S - R\theta)\cos(\theta) + h - S \tag{13}$$

All of these variables are annotated on Figure 10. The tip orientation of the ellipse is computed as:

$$\theta = \operatorname{atan}\left(\frac{-B}{A} \cdot \cot(\tau)\right) - \frac{\pi}{2} \tag{14}$$

Assuming that the coordinates for the arc base at $\tau = 0$ is fixed, the equations can be solved subject to the following equality constraint:

$$h = B \cdot Ellipse(\tau,\ (1 - \tfrac{A^2}{B^2})^{1/2}) \tag{15}$$

where the function *Ellipse* is an incomplete elliptic integral of the second kind. This relationship specifies that the arc length of the ellipse segment must equal the initial notch width *h*, which implies that the neutral axis does not undergo any deformation during bending.

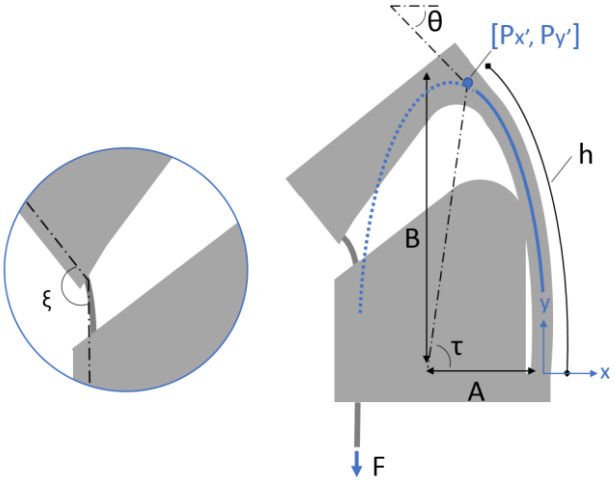

Figure 10: Ellipse Segment Shape Fit

With the shape of the ellipse known, the variation of curvature along its length is computed as:

$$k(t) = \frac{AB}{(A^2\cos(\tau)^2 + B^2 sin(\tau)^2)^{3/2}} \tag{16}$$

where $k(t)$ is the curvature of the neutral axis $\bar{y}$. The curvature of the midline of the tube $k(t)'$ is computed as:

$$k(t)' = \frac{k(t)}{1 - k(t) \cdot \bar{y}} \tag{17}$$

With the curvature known, the force required to articulate the notch to a desired bending angle can be computed by integrating equation (6). However, friction losses from the cable navigating around the corner of a notch must be accounted for. A simple model for this friction loss has been presented in [14]. The actuation force applied on the cable is therefore:

$$F_{cable} = \eta^{2n} F = \left(\frac{\sin(\xi/2) - \mu_s \cos(\xi/2)}{\sin(\xi/2) + \mu_s \cos(\xi/2)}\right)^{2n} F \tag{18}$$

where ξ is the angle between the notch edge and tendon, μ_s is the friction coefficient and *n* is the number of notches making up the overall joint.

5 FABRICATION OF NOTCHED-TUBE JOINT PROTOTYPES

A total of five prototype CCM notched-tube joint specimen were fabricated through laser cutting (Pulse Systems, USA). The performance of this topology was compared to a rectangular notch joint design of equivalent tube radii as well as notch cut depth g, notch height h and notch spacing c, as shown in Figure 11-A. The intent of this comparison is to demonstrate how the behavior of a CCM notch augments the basic notch shape once the contact-aid topology is added to its geometry, effectively comparing $h_i = 0.8$ with $h_i = 0$. The width of the slit feature in the CCM design was limited by the performance of the laser; the smallest width that can be cut is 0.05 mm. Further, because of fabrication constraints, the slits were cut off-axis to the tube at an angle of 15° as shown in Figure 11-B.

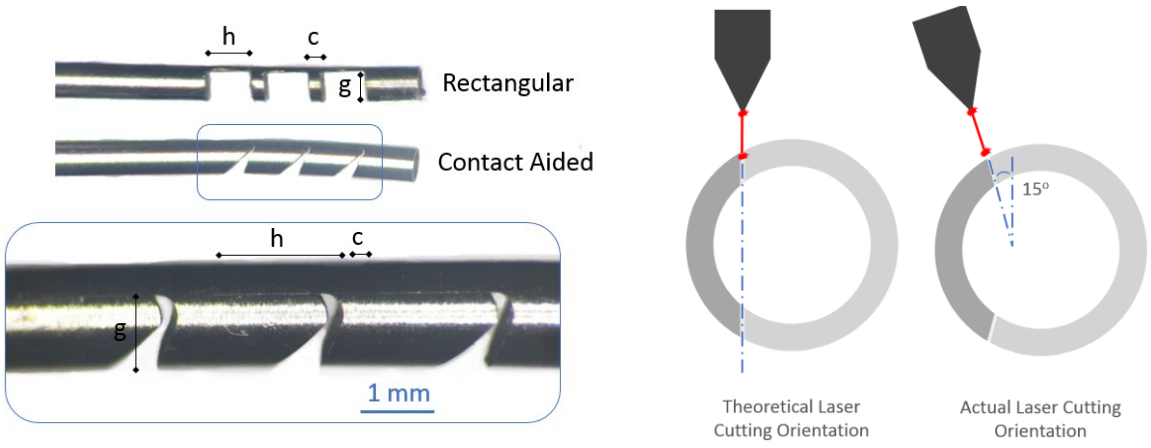

Figure 11: Comparison of Fabricated Rectangular Notch Joint and Joint with Contact-Aid (A). Schematic of Laser Cutting Orientation Used to Construct Test Specimen (B).

6 EXPERIMENTAL METHODS

The range-of-motion of the test specimen were assessed by measuring the tip bending angle as a function of the cable actuation force. Additionally, the stiffness of the joints were assessed by measuring their tip displacements under an applied tip load. The test setup for these experiments were assembled on a ThorLabs optical breadboard fit with manual linear translation

stages (Newport NewFocus, USA) that have 20 µm resolution. These stages were used for the fine alignment of the samples with the force and displacement sensors used to collect the data.

6.1 FORCE-DEFLECTION TESTING

For the tip displacement versus tip-force experiments, an OptoNCDT 1607 time-of-flight laser displacement sensor (Micro-Epsilon, USA) was used to detect the tip's movement and an FSH00091 JR S-Beam Load Cell (FUTEK, USA) was used to measure the blocking force. This experimental set-up is shown in Figure 12-A.

6.2 RANGE-OF-MOTION TESTING

For the tip bending-angle versus cable-actuation-force experiments, a pair of Flea3 1.3 MP cameras (Point Grey, Vancouver Canada) were arranged in a stereo-configuration and calibrated using the MATLAB® Camera Calibration Toolbox. These cameras were used to track the shape, radius of curvature and bending angle of the joints while an FSH00095 JR S-Beam Load Cell (FUTEK, USA) was used to collect cable tension measurements. The error of the measurement system was found to be ± [0.01-0.1] mm in measuring known radii of curvatures in the range of [3-15] mm. This set-up is shown in Figure 12-B.

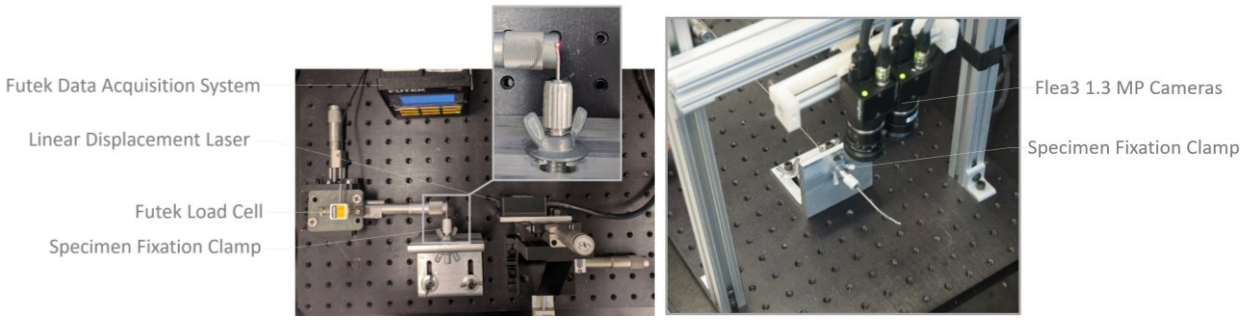

Figure 12: Experimental Set-up for Measuring Blocking Force and Joint Range-of-Motion

7 EXPERIMENTAL ANALYSIS AND MODEL VALIDATION

To verify the anticipated effects of the CCM notches from the sensitivity study in Section 3.2, the physical prototypes were compared against an equivalent rectangular notch design with the same cut depth, g and width, h. This comparison can effectively be considered as $h_i = 0.8$ vs. $h_i = 0$. Figure 13 shows a side-by-side comparison of both simulated and physical versions of the CCM notches alongside a rectangular notch joint. By inspecting these images, it can be seen that the CCM notch takes on a more compact bending shape with less lateral motion. It can also be seen that the ANSYS simulations of these different joints agree well with the true shape of the joints. Note the differences in closure between the distal and proximal joints being accurately represented in the simulations. This validates the cable actuated approach used to simulate the actuation of these joints.

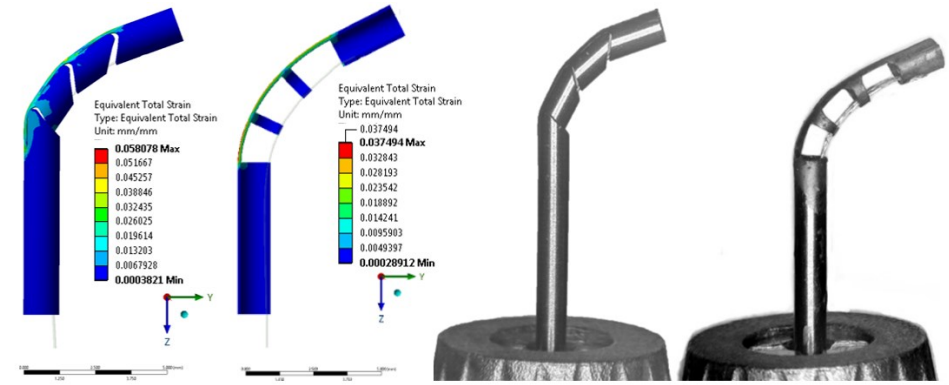

Figure 13: Finite Element and Physical Specimen of Rectangular Joint and Modified Joint

Next, the blocking-force characteristics of the two joints are compared in Figure 14, where the physical experiments were repeated five times for each data point, and the mean and standard error of the measurements are shown.

Both the FEM and experimental data indicate that for a specified “allowable” tip deflection, the CCM design supports blocking forces 1.58 times the magnitude of those applied to the rectangular notch joint.

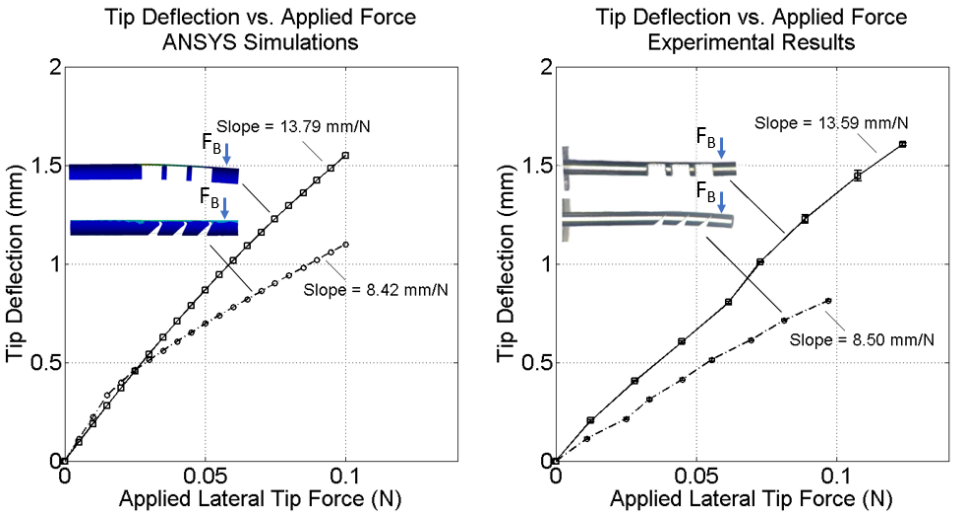

Figure 14: Blocking Force of Rectangular Joint and Contact-aided Joint for ANSYS Simulations and Physical Experiments

The kinematics of the contact-aided joint were also simulated using ANSYS and compared to the analytical model presented in Section 3. These results are compared to experimental data collected from the fabricated specimen in Figure 15.

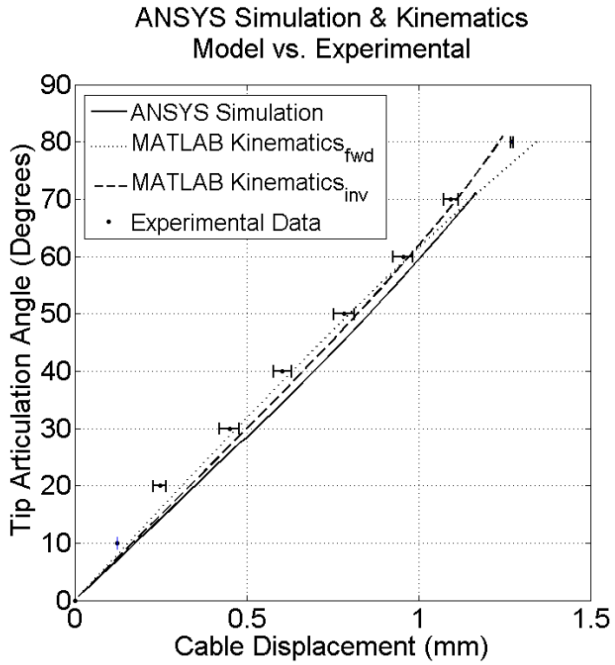

Figure 15: Comparison of Kinematics Model and ANSYS Simulation of CCM Notch Joint with Experimental Results

Figure 16 compares the experimental cable-actuation-force vs bending angle with the ANSYS simulations and the statics model implemented in MATLAB®. Note that the statics model only predicts the forward loading of the joint and does not consider joint unloading. The material parameters used in the statics model are summarized in Table 4. Additionally, the statics model presented in this work was not applied to the rectangular joint geometry in Figure 16-B. The cable actuation vs bending angle results for the equivalent rectangular notch is included for comparison purposes. Note that the cable tension of the CCM notch joint is increased for the same range of motion.

Table 4: Constitutive Model Used with MATLAB Simulation

MATLAB Parameters	Value
Young's Modulus E	55 GPa
Upper Plateau Stress σ_{up}	420 MPa
Lower Plateau Stress σ_{lp}	-420 MPa
Coefficient of Friction μ_s	0.3

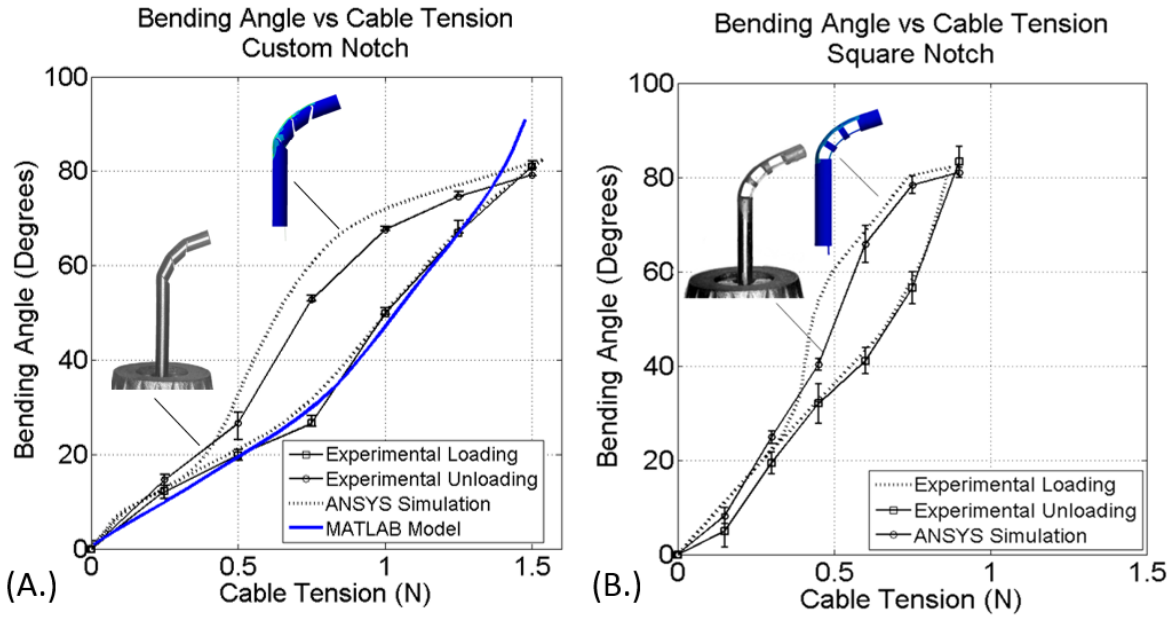

Figure 16: Bending Angle versus Cable Tension for Notched-Tube Prototypes

8 DISCUSSION

Previous work on the design of notch tube compliant joint topologies have proposed the addition of different features into a rectangular notch profile in order to improve its peformance. These features include adding mechanical stops to limit the notch's range-of-motion, filleting the corners of notches to relieve stress concentrations, and progressively increasing the depth to which the notches are cut, from proximal to distal, to create "tip-first-closure". All of these augmentations improve the utility of notched-tube joint mechanisms for miniature manipulation tasks, however, there still remains a significant trade-off between achieving joint compactness and maintaining joint stiffness. In this work, we propose the design of a CCM to aid in increasing the joints' bending stiffness while providing control over the bending shape of the notch. To the best of our knowledge, this design is the first example of a CCM incorportated into a notched-tube compliant joint. We have presented both simulation and experimental results to demonstrate the effect of this modification, and derive a kinematic and statics model to aid with the future incorporation of this mechanism into robotic manipulators. These models have been validated with experimental data.

The CCM notch design was compared to a joint of equivalent size and initial K_1 stiffness, constructed from rectangular notches following the dimensions outlined in Table 1. The purpose of this comparison is to highlight the impact that adding a contact-aid has on the behavior of this equivalently sized notch. This analysis does not consider how the contact-aided topology compares to a rectangular notch that is specifically optimized for stiffness or range-of-motion. The FEM sensitivity study highlights two important benefits of the CCM design. First, the contact-aid increases the bending stiffness of the compliant joint in the loading orientation that is the

most susceptible to large, undesirable deflections from external loads. These large deflections result both from the geometry of asymmetric notches and their material behavior. Nitinol is commonly used for these mechanisms because it has a relatively high elastic strain limit, however, the plateau that occurs in its constitutive model results in a significant loss in stiffness for applied tip loads above a certain threshold, as seen in Figure 7-A. For the particular scales required for neuro-endoscopy, the expected lateral tip forces needed for tissue manipulation are in the 0.1-0.5 N range, which is the same range of tip forces where the plateau affect is seen in the simulations [21], [22]. The CCM geometry can compensate for the stiffness changes brought about by the phase transition from Austenite to Martensite by reinforcing the notch. The second benefit of the CCM design is to change the shape that the compliant region undergoes during bending. For this particular CCM design, the compliant region undertakes an elliptical shape instead of a constant curvature arc which rectangular notches tend toward. This shape change reduces the lateral motion that the joint undergoes when bending which results in a more compact shape which is critical when working in tight spaces. Previous work on designing notches for compact bending focused on tip-first closure, where the depth of cut of each notch could be varied within a set of notches that make up a joint. This concept of varying cut depth could be used to create new cutting patterns that could provide a shape change without a contact aid. However, this approach alone does not address the loss of stiffness of the joint resulting from the cut-outs in the same manner as the CCM notched-tube design. Ultimately, the sensitivity analysis illustrates that the stiffness increase and compactness gained by the CCM design results in strain concentrations around the contact-aid region. This side-effect must be further investigated in future studies.

One of the designs investigated in the sensitivity study was selected and fabricated to validate the FEM results and the models developed in this paper. By inspection, the shape of the joints in Figure 13 show that the CCM notch's overall shape has less lateral motion when compared to its rectangular counterpart, confirming the predictions of the FEM. Further, from Figure 15 we see that both the FEM simulations and the experimental results show an increase in joint stiffness by a factor of approximately 1.6. The FEM simulations depict an initial region where the force-deflection characteristics of the rectangular joint and the augmented joint coincide. This initial deflection occurs before the compliant region makes contact with the contact-aid. Once the self-reinforcement occurs, the slopes of the plots diverge, and the ratio of these new slopes correlate with an increased resistance to externally applied blocking-forces. Differences between the FEM and experimental figures can be accounted for based on the shape of the physical specimen under no loading. The laser cut CCM notches experienced excessive thermal effects during their manufacturing which resulted in plastically deforming the notches such that in their resting state the compliant region is already touching the contact-aid. This caused the plots for the experimental data to diverge immediately. Overall, the CCM design improves the effective stiffness K of the joint throughout nearly its full range of motion as desired. This effect is distinct from tapering the notch edges to create mechanical closure in that the joint's stiffness only increases when the notch closes at maximum bending.

The results comparing the cable tension vs. bending angle presented in Figure 16 indicate that both the rectangular and contact-aided joint are capable of articulating through the same range-of-motion, which is a bending angle of approximately 80^{o}. The primary difference between the two loading-unloading curves is the cable tension required to articulate the joints. The

tensions required for the augmented joint are approximately double those required for the rectangular joint. Ideally, the contact-aid would only impact the stiffness of the joint against externally applied loads and would have negligible effects on the required cable actuation forces. However, the actuation cables used to articulate joints of this size are capable of supporting loads an order of magnitude higher than these values, and therefore, we expect the increase in cable tension to be manageable for many design variations. Figure 16 also highlights the agreement between the statics model, FEM model and experimental results. In both cases, the constitutive model and coefficient of friction used were the same. The FEM simulation and experimental data for the rectangular asymmetric notch joint in Figure 16-B also aligns very well. Both of these cases provide support that the FEM simulations are an effective predictive design tool for the future development of these mechanisms.

The experimental set-ups depicted in Figure 12 which were used to measure the joint's stiffness and range-of-motion had the following limitations. First, alignment of the samples within the specimen fixation clamp was done manually and therefore the samples were not aligned perfectly orthogonal to the plane of the optical breadboard. To address this limitation, a stereo-camera measurement system was used instead of a single planar camera to capture out-of-plane bending. The measurement errors for radius of curvature, joint arc length and joint angle were quantified by conducting control measurements of twenty sample arcs machined into an aluminum plate. Each arc measurement was repeated five times, and the error ranged from ± [0.01-0.1] mm in measuring known radii of curvatures in the range of [3-15] mm.

Considering the kinematics model, one of its limitations is the assumption that the majority of bending occurs at the contact region. Based on the results of Figure 15, this

assumption holds for the present contact-aid geometry, however agreement with the model may decline as the maximum articulation angle increases above the set-point of 30^{o}. The model also assumes that the compliant region wraps around the fillet radius of the contact region, and as this radius is reduced below the current design of 0.2 mm, this behavior may change.

The most significant limitation of the statics model is that in its present form, it does not incorporate the hysteresis present in nitinol. Therefore, it only models loading of the joint and not unloading. Further, the shape estimation of the notch elliptical arc is contingent on the accuracy of the kinematics model.

This study has presented a new design strategy for developing stiff and compact notched-tube joints. Future work on this subject will focus on applying topological optimization techniques such as evolutionary or genetic algorithms to the design of these CCM [23]–[25]. These tools can be used to critically assess the chosen shape, and consider the impact of the design parameters that were held fixed in this study, such as the edge taper angles. A more global topology optimization may also be able to answer whether a multi-point contact-aid may provide additional performance benefits compared to the single-point contact-aid presented here.

9 CONCLUSION

Here we present an overview of the design of a novel notched-tube contact-aided compliant joint, with a particular emphasis on applications in small workspaces, specifically minimally invasive neurosurgery. This contact-aided design prototype increases the joint's blocking-forces and allows for more compact designs to be developed. The improvements in compactness are achieved by reducing the lateral displacement of the joint when bending and allowing for the use of fewer, longer notch joints which will achieve a desired bending angle while

the joint itself occupies a smaller footprint. Future work will focus on the topological optimization of the joint for an application specific task.

10 REFERENCES

[1] P. A. York, P. J. Swaney, H. B. Gilbert, and R. J. Webster III, "A Wrist for Needle-Sized Surgical Robots," in *IEEE International Conference on Robotics and Automation*, 2015, pp. 1776–1781.

[2] P. J. Swaney, P. A. York, H. B. Gilbert, J. Burgner-Kahrs, and R. J. Webster III, "Design, Fabrication, and Testing of a Needle-sized Wrist for Surgical Instruments," *ASME J. Med. Devices*, no. c, 2016.

[3] K. W. Eastwood, H. Azimian, B. Carrillo, T. Looi, H. E. Naguib, and J. M. Drake, "Kinetostatic Design of Asymmetric Notch Joints for Surgical Tools," in *2016 IEEE/RSJ International Conference on Intelligent Robots and Systems (IROS 2016*, 2016, p. Accepted.

[4] T. Kato, I. Okumura, H. Kose, K. Takagi, and N. Hata, "Extended Kinematic Mapping of Tendon-Driven Continuum Robot for Neuroendoscopy," no. Iros, pp. 1997–2002, 2014.

[5] F. Dewaele, a. F. Kalmar, F. De Ryck, N. Lumen, L. Williams, E. Baert, H. Vereecke, J. P. Kalala Okito, C. Mabilde, B. Blanckaert, V. Keereman, L. Leybaert, Y. Van Nieuwenhove, J. Caemaert, and D. Van Roost, "A Novel Design for Steerable Instruments Based on Laser-Cut Nitinol," *Surg. Innov.*, vol. 21, no. 3, pp. 303–311, 2014.

[6] M. Mitsuishi, P. Bartolo, Y. Kanada, T. Yoneyama, T. Watanabe, H. Kagawa, N. Sugiyama, K. Tanaka, and T. Hanyu, "Force feedback manipulating system for neurosurgery," *First CIRP Conf. BioManufacturing*, vol. 5, no. 1, pp. 133–136, 2013.

[7] T. Yoneyama, T. Watanabe, H. Kagawa, J. Hamada, Y. Hayashi, and M. Nakada, "Force detecting gripper and flexible micro manipulator for neurosurgery.," *Conf. Proc. IEEE Eng. Med. Biol. Soc.*, vol. 2011, pp. 6695–9, Jan. 2011.

[8] K. W. Eastwood, V. P. Bodani, and J. M. Drake, "Three-Dimensional Simulation of Collision Free Paths for Combined Endoscopic Third Ventriculostomy and Pineal Region Tumor Biopsy: Implications for the Design Specifications of Future Flexible Endoscopic Instruments," *Oper. Neurosurg.*, 2015.

[9] J. A. Bell, C. E. Saikus, K. Ratnayaka, V. Wu, M. Sonmez, A. Z. Faranesh, J. H. Colyer, R. J. Lederman, and O. Kocaturk, "A Deflectable Guiding Catheter for Real-Time MRI-Guided Interventions," *J. Magn. Reson. Imaging*, vol. 35, no. 4, pp. 908–915, 2012.

[10] H. Fischer, B. Vogel, W. Pfleging, and H. Besser, "Flexible distal tip made of nitinol (NiTi) for a steerable endoscopic camera system," *Mater. Sci. Eng. A*, vol. 273–275, pp. 780–783, 1999.

[11] Y. Haga, Y. Muyari, S. Goto, T. Matsunaga, and M. Esashi, "Development of Minimally Invasive Medical Tools Using Laser Processing on Cylindrical Substrates," *Electr. Eng. Japan*, vol. 176, no. 1, pp. 65–74, 2011.

[12] J. Peirs, H. Van Brussel, D. Reynaerts, and G. De Gersem, "A Flexible Distal Tip with Two Degrees of Freedom for Enhanced Dexterity in Endoscopic Robot Surgery," in *The 13th Micromechanics Europe Workshop*, 2002, pp. 271–274.

[13] S. C. Ryu, P. Renaud, R. J. Black, B. L. Daniel, and M. R. Cutkosky, "Feasibility Study of an Optically Actuated MR-compatible Active Needle," in *IEEE International Conference on Intelligent Robots and Systems*, 2011, pp. 2564–2569.

[14] A. Gao, R. Murphy, H. Liu, I. Iordachita, and M. Armand, "Mechanical Model of Dexterous Continuum Manipulators with Compliant Joints and Tendon/External Force Interactions," *IEEE/ASME Trans. Mechatronics*, 2016.

[15] M. D. M. Kutzer, S. M. Segreti, C. Y. Brown, R. H. Taylor, S. C. Mears, and M. Armand, "Design of a New Cable-Driven Manipulator with a Large Open Lumen: Preliminary Applications in the Minimally-Invasive Removal of Osteolysis," in *IEEE International Conference on Robotics and Automation*, 2011, pp. 2913–2920.

[16] J. Liu, B. Hall, M. Frecker, and E. W. Reutzel, "Compliant articulation structure using superelastic NiTiNOL," *Smart Mater. Struct.*, vol. 22, no. 9, 2013.

[17] J. Peirs, H. Van Brussel, D. Reynaerts, and G. De Gersem, "A Flexible Distal Tip with Two Degrees of Freedom for Enhanced Dexterity in Endoscopic Robot Surgery," in *The 13th Micromechanics Europe Workshop*, 2002,

pp. 271–274.

[18] D. Wei, Y. Wenlong, H. Dawei, and D. Zhijiang, “Modeling of Flexible Arm with Triangular Notches for Applications in Single Port Access Abdominal Surgery,” in *IEEE International Conference on Robotics and Biomimetics*, 2012, pp. 588–593.

[19] N. Lobontiu, M. Cullin, T. Petersen, J. a Alcazar, and S. Member, “Planar Compliances of Symmetric Notch Flexure Hinges : The Right Circularly Corner-Filleted Parabolic Design,” vol. 11, no. 1, pp. 169–176, 2014.

[20] J. R. Cannon and L. L. Howell, “A compliant contact-aided revolute joint,” *Mech. Mach. Theory*, vol. 40, no. 11, pp. 1273–1293, 2005.

[21] H. J. Marcus, K. Zareinia, L. S. Gan, F. W. Yang, S. Lama, G.-Z. Yang, and G. R. Sutherland, “Forces exerted during microneurosurgery: a cadaver study,” *Int. J. Med. Robot. Comput. Assist. Surg.*, 2014.

[22] J. R. Bekeny, P. J. Swaney, R. J. Webster, P. T. Russell, and K. D. Weaver, “Forces Applied at the Skull Base during Transnasal Endoscopic Transsphenoidal Pituitary Tumor Excision,” *J. Neurol. Surg. - Part B*, vol. 74, no. 6, pp. 337–41, Dec. 2013.

[23] P. A. Halverson and A. E. Bowden, “A FLEXURE-BASED BI-AXIAL CONTACT-AIDED COMPLIANT MECHANISM FOR SPINAL ARTHROPLASTY,” *Proc. ASME 2008 Interational Des. Eng. Tech. Conf.*, 2008.

[24] Y. Tummala, A. Wissa, M. Frecker, and J. E. Hubbard Jr., “Design and Optimization of a Contact-Aided Compliant Mechanism for Passive Bending,” *J. Mech. Robot.*, vol. 6, no. 031013, pp. JMR–13–1179, 2014.

[25] M. Frecker and G. A. Lesieutre, “TOPOLOGY OPTIMIZATION OF CONTACT-AIDED COMPLIANT CELLULAR MECHANISMS,” *Proc. ASME 2009 Conf. Smart Mater. Adapt. Struct. Intell. Syst.*, 2009.